# ARTICLE   OPEN

Check for updates

# Efficient quantum information probes of nonequilibrium quantum criticality

Miguel M. Oliveira [1✉], Pedro Ribeiro [1,2✉] and Stefan Kirchner [3,4✉]

Quantum information-based approaches, in particular the fidelity, have been flexible probes for phase boundaries of quantum matter. A major hurdle to a more widespread application of fidelity and other quantum information measures to strongly correlated quantum materials is the inaccessibility of the fidelity susceptibility to most state-of-the-art numerical methods. This is particularly apparent away from equilibrium where, at present, no general critical theory is available and many standard techniques fail. Motivated by the usefulness of quantum information-based measures we show that a widely accessible quantity, the single-particle affinity, is able to serve as a versatile instrument to identify phase transitions beyond Landau's paradigm. We demonstrate that it not only is able to signal previously identified nonequilibrium phase transitions but also has the potential to detect hitherto unknown phases in models of quantum matter far from equilibrium.

## INTRODUCTION

Quantum fluctuations drive zero temperature quantum phase transitions[1]. In equilibrium, the fluctuation-induced long-range entanglement has been successfully used as a probe of quantum criticality[2,3].

Away from equilibrium, the situation seems less clear. Quantum systems far from equilibrium can exhibit a wide variety of phenomena ranging from the usual symmetry-based phase transitions[4–13] to the more exotic behavior, such as mixed-order phase transitions[14–16] or time crystallinity[17,18], with no equilibrium counterpart. Probing such systems necessarily requires an understanding of their nonequilibrium properties. While a general theory of far-from-equilibrium criticality is not available, it is known that not all systems are describable in terms of order parameter fluctuations[19]. Already the mere detection of a phase transition away from equilibrium, where thermodynamic minimization principles no longer apply, can be challenging, in particular if the order parameter is elusive. Likewise, detecting phase transitions based on spectral properties require information on excited states that is also hard to access by most methods.

Quantum information-centered approaches, based on the fidelity, are natural candidates as "all purpose" quantities to circumvent that issue, i.e., to detect phase transitions in the absence of additional knowledge[20–24]. However, for interacting many-body systems its computation requires information about the full-density matrix. This makes it forbiddingly difficult, if not impossible, to compute the fidelity as most state-of-the-art numerical techniques only allow for the faithful determination of few-body observables. This renders the fidelity inaccessible to Quantum Monte Carlo methods and rescinds the advantage of the exponential compression exploited by variational methods such as the density matrix renormalization group (DMRG) for mixed states.

Single-particle correlators, which form the basic building block of many-body theory, are in contrast readily accessible. In equilibrium, the use of the single-particle correlator matrix was

first proposed in the context of the superfluidity transition[25]. Similar methods have recently been employed to test for many-body localization in closed systems[26,27]. Thus, the idea of extending quantum information concepts, in particular the fidelity, to single-particle observables as a versatile tool to detect phase transitions away from equilibrium presents itself.

Here, we provide a proof-of-concept of this idea by establishing that a class of single-particle observables, referred to as single-particle distances, can detect phase transitions out of equilibrium. These quantities are derived from a notion of proximity between quantum states. Being dependent solely on single-particle quantities, these distances can be efficiently evaluated by commonly employed numerical methods. We demonstrate that they can be used in the detection of phase transitions between mixed states, arising in open quantum system setups and also in equilibrium at finite temperatures. This observation is particularly pertinent in the out-of-equilibrium case due to a lack of alternative methods. In what follows, we focus on the single-particle affinity (SPA) defined below, which exactly reduces the fidelity for Gaussian states.

We illustrate the usefulness of the SPA through the discussion of a model with a well-established non-equilibrium steady-state (NESS) phase diagram. We then apply the SPA as an "all purpose" detector of phase transitions using it to investigate a boundary-driven fermionic ladder whose NESS phase diagram has not been reported so far. As it turns out, this phase diagram is rather rich, contrary to naive expectations. This thus establishes the usefulness of the SPA. We also confirm the findings based on the SPA through a careful analysis of the finite size scaling of the current.

## RESULTS

### Single-particle affinity

In order to assess the far-from-equilibrium behavior of electronic matter, we note that for a fermionic system all single-particle observables can be obtained from the covariance matrix $\Sigma = \langle \mathbf{C}$

[1]CeFEMA, Instituto Superior Técnico, Universidade de Lisboa, Av. Rovisco Pais, 1049-001 Lisboa, Portugal. [2]Beijing Computational Science Research Center, Beijing 100193, China. [3]Department of Electrophysics, National Yang Ming Chiao Tung University, Hsinchu 30010, Taiwan, ROC. [4]Center for Emergent Functional Matter Science, National Yang Ming Chiao Tung University, Hsinchu 30010, Taiwan, ROC. ✉email: miguel.m.oliveira@tecnico.ulisboa.pt; ribeiro.pedro@tecnico.ulisboa.pt; stefan.kirchner@correlated-matter.com

$\mathbf{C}^\dagger\rangle$, where $\mathbf{C} = \left(c_1, c_2, \cdots, c_1^\dagger, c_2^\dagger, \cdots\right)^T$ is a Nambu-vector. Here, $\boldsymbol{\Sigma}$ is Hermitian, $\boldsymbol{\Sigma}^\dagger = \boldsymbol{\Sigma}$ and respects charge conjugation symmetry, i.e., $\boldsymbol{\Sigma} = \tau_x(1 - \boldsymbol{\Sigma}^T)\tau_x$, with $\tau_x$ being the $x$ Pauli matrix acting in Nambu space.

It is well known that in equilibrium, the order parameter of, e.g., charge-, spin-density waves, or superconducting phases is constructed from single-particle operators, which can even signal topological phase transitions for which a local order parameter cannot be defined. Even far from equilibrium, where a symmetry-breaking order parameter is often not available, the covariance matrix may still encode important information about phase changes in the NESS.

We explore the ability of the covariance matrix to identify phase transitions by studying a suitable measure of distance between covariance matrices $D_{\mathcal{A}}(\boldsymbol{\Sigma}_1, \boldsymbol{\Sigma}_2) = \sqrt{2 - 2\sqrt{\mathcal{A}(\boldsymbol{\Sigma}_1, \boldsymbol{\Sigma}_2)}}$ where $\mathcal{A}$ is a quantity we will refer to as SPA. It is defined by

$$\mathcal{A}(\boldsymbol{\Sigma}_1, \boldsymbol{\Sigma}_2) = \frac{\det\left[\mathbf{1} + \sqrt{(1 - \mathbf{1}\boldsymbol{\Sigma} - \mathbf{1})(2 - \mathbf{1}\boldsymbol{\Sigma} - \mathbf{1})}\right]}{\sqrt{\det[\mathbf{1} - \mathbf{1}\boldsymbol{\Sigma}]\det[2 - \mathbf{1}\boldsymbol{\Sigma}]}}. \tag{1}$$

$D_{\mathcal{A}}$ possesses all the properties of a metric, thus providing a sensible notion of affinity between two states (see the Methods section). For noninteracting systems the density matrices are Gaussian, in which case $\mathcal{A}$ coincides with the fidelity $F$, i.e., $F(\rho_1, \rho_2) = \mathcal{A}(\boldsymbol{\Sigma}_1, \boldsymbol{\Sigma}_2)$, where $F(\rho_1, \rho_2) = \left(\text{Tr}\sqrt{\sqrt{\rho_1}\rho_2\sqrt{\rho_1}}\right)^2$ and $\boldsymbol{\Sigma}_i = \text{Tr}\left[\mathbf{C}\mathbf{C}^\dagger\rho_i\right]$. Therefore, in the quadratic case $D_{\mathcal{A}}(\boldsymbol{\Sigma}_1, \boldsymbol{\Sigma}_2)$ reduces to the Bures distance $D_{\mathcal{B}}(\rho_1, \rho_2) = \sqrt{2 - 2\sqrt{F(\rho_1, \rho_2)}}$[28–31].

As the quantities entering $\boldsymbol{\Sigma}$ are, at least in principle, straightforwardly accessible in most numerical and approximation methods, detecting phase-transitions based on this quantity is of great practical relevance. This is in contrast to the fidelity whose numerical calculation, for an interacting system, is in general not feasible. To address this issue, we demonstrate the usefulness of $\mathcal{A}$ for detecting steady-state phase transitions of interacting systems which can be evaluated efficiently. This is accomplished by studying a generalized linear response susceptibility associated with $\mathcal{A}$ and defined through

$$\mathcal{A}[\boldsymbol{\Sigma}(\boldsymbol{\lambda}), \boldsymbol{\Sigma}(\boldsymbol{\lambda} + \boldsymbol{d}\lambda)] = 1 - \sum_{i,j} \chi_{\mathcal{A}}^{i,j}(\boldsymbol{\lambda}) \frac{d\lambda_i \, d\lambda_j}{2} + O(d\lambda^3), \tag{2}$$

where $\boldsymbol{\lambda}$ parametrizes the NESS. Here, the first derivative term is absent since the expansion is done around the maximum. By construction, $\mathcal{A}$ reproduces previous results for non-interacting fermionic systems based on $F$[21] and $\chi_{\mathcal{A}}^{i,j}$ reduces to the fidelity susceptibility.

## Application to boundary driven systems

The methodology proposed here is applicable to open quantum systems. An important subset of those are systems in the so-called Markovian regime on which we focus in what follows. Within the Markovian approximation, time scales of the environment are taken to be much shorter than those of the system. This Markovian limit has recently received considerable attention[32] both for its physical relevance and because it represents a substantial simplification with respect to generic open many-body quantum systems. Additionally, for a wide class of one-dimensional models, non-equilibrium steady-states (NESS) of Markovian systems can be effectively parameterized by matrix product operators (MPO)[33–38]. This approach leads to a number of important developments for the transport properties of quantum systems and in particular spin chains. For a boundary-driven Heisenberg XXZ chain, e.g., it helped establish the NESS phase

diagram[39–47]. Further support came from a series of exact results[48–52].

We consider two boundary-driven models with Markovian reservoirs that allow injection or removal of electrons. The Markovian evolution is described by a Lindblad equation[53,54]

$$\partial_t \rho = \mathcal{L}(\rho), \tag{3}$$

where $\rho$ is the density matrix of the system. The Lindblad operator $\mathcal{L}$ is given by

$$\mathcal{L}(\rho) = -i[H, \rho] + \sum_\alpha \left( W_\alpha^\dagger \rho W_\alpha - \frac{1}{2}\left\{W_\alpha^\dagger W_\alpha, \rho\right\} \right). \tag{4}$$

Here [] and {} denote commutator and anti-commutator respectively, while $W_l$ is the so-called jump operators which encode the system-reservoir couplings. In Eq. (4), the first term is responsible for the unitary part of the time evolution and the second describes driving and dissipation.

We analyze the steady-state properties of the models defined below using techniques for open systems based on MPS, which have been shown to yield reliable results for this class of boundary-driven problems[33,34]. Starting in the infinite temperature state, we time evolve the system according to Eq. (4) using the t-DMRG algorithm[55] until it reaches the steady state. Details of the implementation and convergence of the algorithm are provided in the Methods section and the Supplementary Note 4. Except when explicitly stated otherwise, all numerical results were obtained using matrix product state (MPS) techniques[33,34,39].
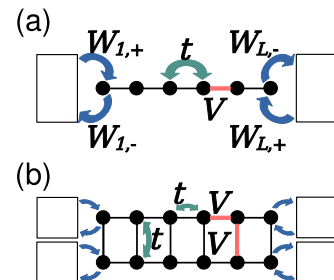
## Fermionic chain

The first system we consider is the $t - V$ model for spinless electrons on a chain. We demonstrate that $\mathcal{A}$ reproduces the previously known phase diagram. A sketch of the model is provided in Fig. 1a and its Hamiltonian is given by (see also (7) of Method section)

$$H = \sum_{\langle i,j\rangle} \left[ -t \, c_i^\dagger c_j + \frac{V}{2}\left(n_i - \frac{1}{2}\right)\left(n_j - \frac{1}{2}\right) \right], \tag{5}$$

where $c_i^\dagger, c_i$ are the creation and annihilation operators on site $i$, $n_i = c_i^\dagger c_i$, $t$ is the hopping amplitude, set to unity in the following, $V$ is a nearest-neighbor density-density interaction and $L$ the length of the system. Here, $i = 1, ..., L$, and the nearest neighbor summation, $\sum_{\langle i,j\rangle}$, is restricted to $j = i \pm 1$, where open boundary conditions are assumed. The jump operators in this case are

$$W_{l,-} = \sqrt{\Gamma_l \frac{1 - \eta_l}{2}} c_l, \quad W_{l,+} = \sqrt{\Gamma_l \frac{1 + \eta_l}{2}} c_l^\dagger, \tag{6}$$

where $l = 1, L$ labels the endpoints of the chain, $\Gamma_l$ is the injection/removal rate for the $l$th reservoir and the bias $\eta_l$ specifies the associated imbalance between particle injection and removal. Thus, the summation in Eq.(4) is performed over $\alpha = (l, \pm)$. In what follows we set $\Gamma_l = 1$ and reduce the bias to a single parameter



**Fig. 1 Schematics of the studied models.** Fermion chain (**a**) and fermion ladder (**b**).
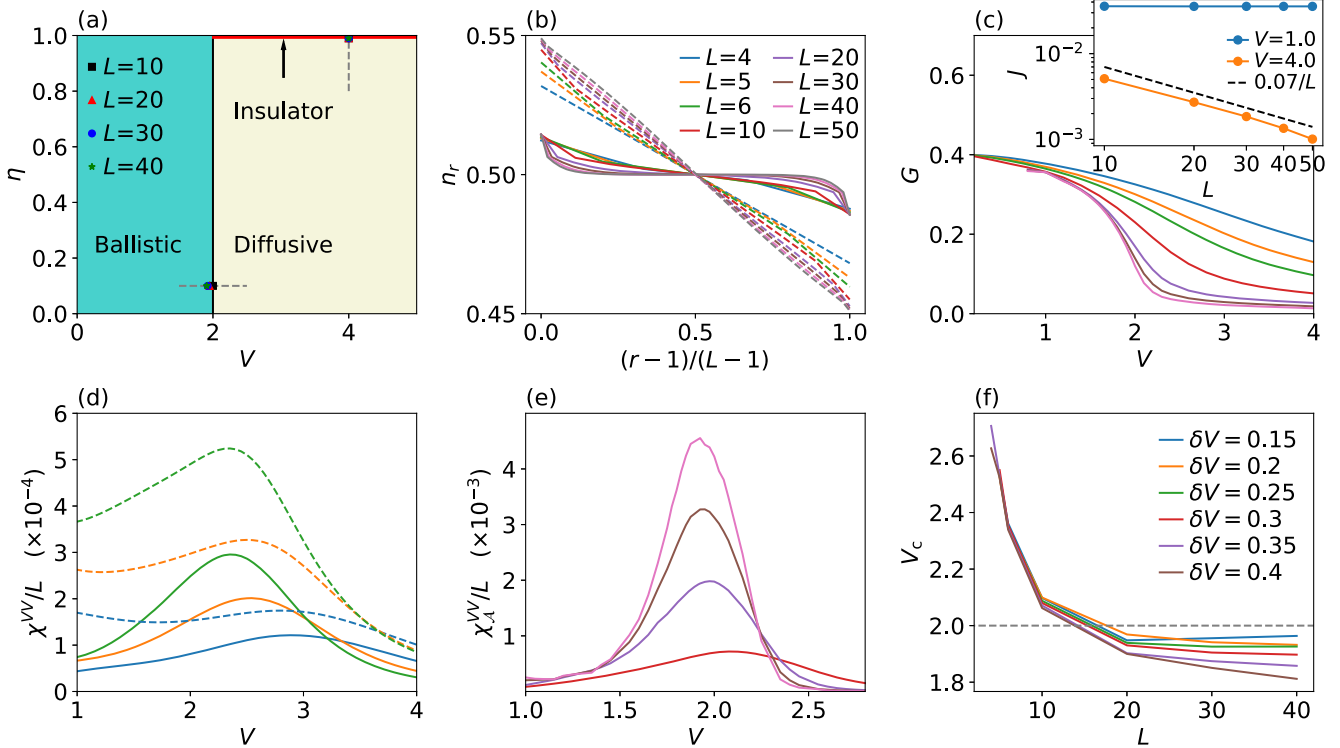
**Fig. 2 Results for the fermionic chain. a** Sketch of the known phase diagram, showcasing a ballistic, diffusive, and insulating regimes. The symbols give the location of the peaks in **e** for different system sizes. **b** Comparison of the real space occupations between the ballistic phase at $V = 1.0$ (continuous) and the diffusive at $V = 4.0$ (dashed). Figures **b**–**f** are obtained for $\eta = 0.1$. Figures **b**–**e** use the color code given in **b**. **c** $G$ versus $V$ for different system sizes. Inset shows the current's dependence with $L$ for the different regimes, with the dashed line being a guide for the eyes delineating the diffusive behavior. **d** Comparison of affinity (continuous) and fidelity (dashed) susceptibilities per degree of freedom obtained by exact diagonalization for $\delta V = 0.01$. **e** $\chi_{\mathcal{A}}^{VV}/L$ for $\delta V = 0.2$ obtained via MPS. **f** Critical coupling $V_c$, measured as maximum of $\chi_{\mathcal{A}}^{VV}$ vs $L$ for different perturbation sizes.

$\eta_1 = -\eta_L = \eta$. As a result, Eq. (5) is equivalent to the boundary-driven XXZ chain studied in refs. [39–47,50,51].

The steady-state phase diagram of the boundary-driven $t - V$ chain model is reproduced in Fig. 2a. Figure 2b shows the real space occupations, $n_r = c_r^\dagger c_r$. In the diffusive regime, away from the boundaries, the density profile is linear in $r$, i.e., $n_r - 1/2 \propto \eta(1/2 - r/L)$. This is in contrast to the ballistic case where the density profile is position independent away from the leads[39–41]. The diffusion constant is then defined as $J = -D(V, \eta)\frac{\partial n_r}{\partial r}$, and becomes independent of $\eta$ for small $\eta$.

Figure 2c (inset) depicts the dependence of the current $J(L) = -it\left\langle c_i^\dagger c_{i+1} - \text{h.c.} \right\rangle$ on $L$ in each of the phases: the ballistic phase, for $V < V_c = 2$, where $J(L)$ is $L$ independent; the diffusive regime where $J(L) \propto L^{-1}$; and the insulating phase (not shown) for $\eta = 1$ and $V > V_c$ where $J(L)$ vanishes exponentially with $L$[41].

This leads us to the identification of a suitable order parameter to distinguish the possible regimes. We make use of the change of behavior of the current – $L$-independent in the ballistic and ~$1/L$ in the diffusive regime—to introduce the conductance $G = J/\eta$, where $\eta$ takes the place of the applied bias. This quantity is shown in Fig. 2c (main panel).

Given both the relative simplicity and the existence of many reliable results make this model an ideal benchmark for our method. Figure 2d, e shows the SPA susceptibility, $\chi_{\mathcal{A}}^{VV} \simeq -\delta V^{-2}[\mathcal{A}(V + \delta V) - 2\mathcal{A}(V) + \mathcal{A}(V - \delta V)]$ (see Eq. (2)), for the well-established ballistic-diffusive transition of the chain model. Figure 2d also depicts a comparison with the fidelity susceptibility, $\chi_F^{VV}$, for small systems sizes, obtained by exact diagonalization. Clearly $\chi_F^{VV}$ signals the presence of a transition of the infinite

system, at $V_c$, already for reduced system sizes and $\chi_{\mathcal{A}}^{VV}$ tracks the behavior of $\chi_F^{VV}$ near the transition.

Figure 2f shows the position of the maximum of $\chi_{\mathcal{A}}^{VV}$ as a function of $L$ for different perturbation sizes $\delta V$. The finite-size scaling analysis confirms that $\chi_{\mathcal{A}}^{VV}$ can be used to effectively detect the steady-state phase transition located at $V_c = 2$. The finite-size scaling analysis for fixed $\delta V$ leads to a $V_c(\delta V) < V_c$ which approaches $V_c$ as $\delta V$ decreases, i.e., $V_c(\delta V \to 0) \to V_c$. In practice, a decrease in $\delta V$ needs to be balanced against the concomitantly increasing computational effort.

We checked that the critical phase boundary in Fig. 2a at $\eta = 1$ is also detected by the proper affinity susceptibility, $\chi_{\mathcal{A}}^{\eta\eta}$, both for the critical insulating phase ($V > V_c$) and for the critical ballistic phase ($V < V_c$) (see Supplementary Note 2).

## Fermionic ladder

The second case we consider is that of an interacting two-leg ladder whose NESS behavior has so far not been addressed. A sketch of the model is shown in Fig. 1b. The system is described by Eq. (5), with $i = (r, \tau)$, where $r = 1, ..., L$ labels the rungs and $\tau = 1, 2$ the legs. Hopping and interactions are restricted to nearest-neighbors of the ladder geometry. The jump operators, located at the ends of the ladder, are given by Eq. (6) with $l = (r = 1, L; \tau = 1, 2)$, $\eta_{(r=1, \tau=1, 2)} = -\eta_{(r=L, \tau=1, 2)} = \eta$ and $\Gamma_{(r=1, L, \tau=1, 2)} = 1$. The full Hamiltonian governing the dynamics of this model is provided in (8) of the method section.

Related systems featuring spins on a ladder were studied by Žnidarič[56,57]. The Hubbard model which can also be seen as a ladder system with the spin projection as the leg index has been widely studied[58–60]. It was found that, in contrast to the chain, the
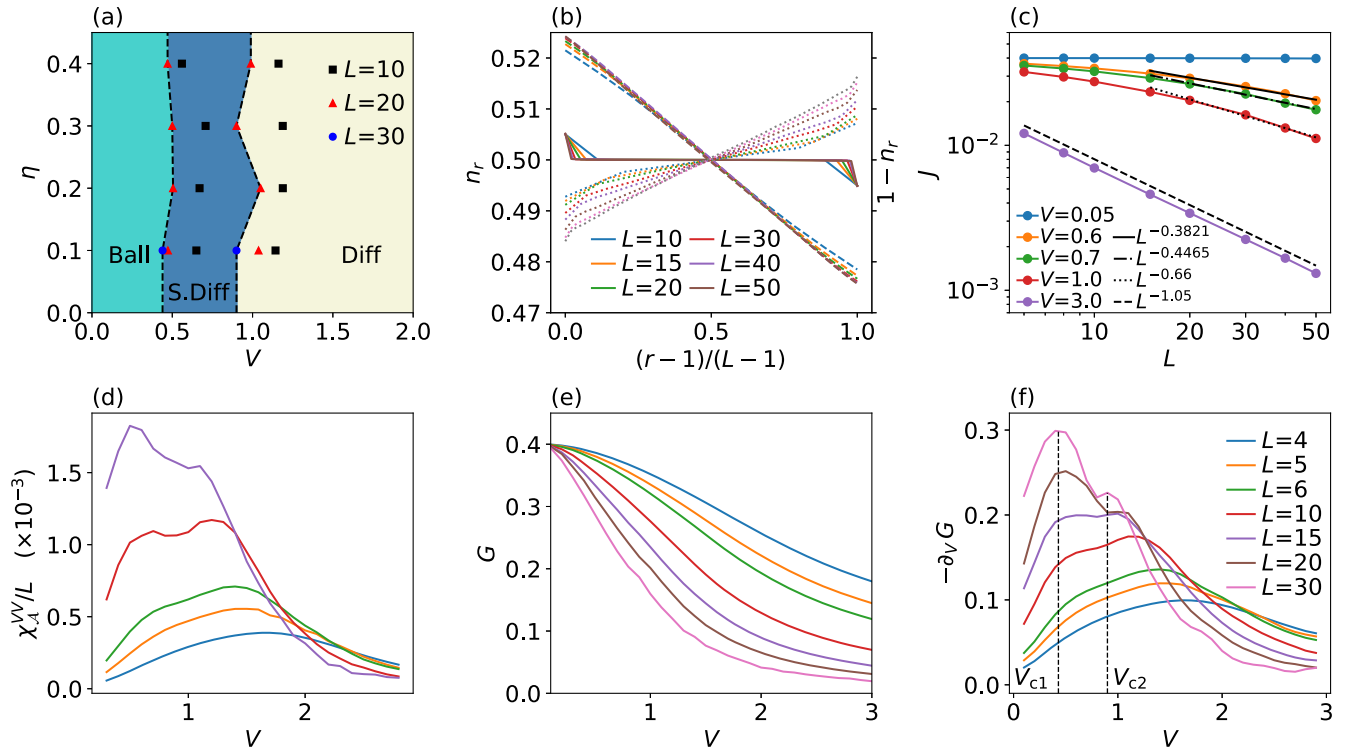
**Fig. 3 Results for the fermionic ladder. a** Tentative finite-sized phase diagram, showing a ballistic (Ball), diffusive (Diff), and super-diffusive (S. Diff) regimes. Phase boundaries lines are based on the largest converged system size. The symbols give the location of the peaks in **f** for different system sizes showcasing the drift of $V_{c1}$ and $V_{c2}$. **b** Comparison of the real space occupations between the ballistic phase at $V = 0.05$ (continuous), the diffusive at $V = 3.0$ (dashed) and the super-diffusive at $V = 0.7$ (dotted); all for $\eta = 0.05$. For the super-diffusive case (dotted) we showed $1 - n_r$ to avoid overlapping the curves. **c** Comparison of the $L$ dependence of the current for the different regimes, with $\eta = 0.05$. The straight lines serve as guides to the eye for the power-law behavior of the diffusive and super-diffusive phases. **d** $\chi_{\mathcal{A}}^{VV}/L$ vs $V$ for different system sizes at $\eta = 0.1$ and with $\delta V = 0.2$, detecting a transition from a ballistic to a diffusive phase, while crossing an intermediate super-diffusive regime. The color code for figures **d**–**f** is given in **f**. **e** and **f** showcase $G$ and $-\partial_V G$ (finite differences) vs $V$ for different $L$ and $\eta = 0.1$, with the result in **f** smoothed with a low-pass filter to remove high-frequency noise.

ballistic regime appears to be absent for locally coupled reservoirs under symmetric driving. Generic diffusive behavior was also found for closed spin ladders in the linear-response regime using quantum typicality arguments[61].

Motivated by the results of refs. [56–58] one may expect that the phase diagram of the fermionic ladder would feature only diffusive behavior. This expectation, however, is in contrast to the behavior of the $\chi_{\mathcal{A}}^{VV}$ vs. $V$, shown in Fig. 3d for different $L$. As $L$ increases, this quantity develops a two-peak structure hinting at the existence of two phase transitions, located at $V_{c1}$ and $V_{c2}$, and a much richer phase diagram.

To further demonstrate the predictive power of $\Sigma$ we turn to a discussion of the properties of the different regimes. In Fig. 3c, we show $J$ as a function of $L$. Surprisingly, in addition to the ballistic and diffusive phases for small and large $V$, respectively, we find a super-diffusive regime at intermediate $V$ for which $J \propto L^{-\nu}$, with $0 < \nu < 1$.

Figure 3b shows the density profiles for the three phases in one of the legs of the ladder. The profiles in the ballistic and diffusive regimes have a behavior which is reminiscent of the corresponding phases of the chain. For the super-diffusive phase, the density profile also seems to depend linearly in $r$ near the middle of the system.

Figure 3a depicts the phase diagram calculated from the maxima of $-\partial_V G$, shown in Fig. 3f, computed from the conductance in Fig. 3e. We note that, although our results point to the existence of three distinct phases, we observe a small drift of the critical value of $V_{c1}$ and $V_{c2}$ with system size. At the present stage, we thus cannot completely rule out that in the infinite

system limit the $V_{c1} \to 0$, i.e., ballistic transport only arises at $V = 0$, or even a more dramatic scenario where both $V_{c1}, V_{c2} \to 0$ and only the diffusive phase is stable for finite $V$. Although unlikely, disproving these scenarios will require further studies. Either way, what is important in the present context is that $\chi_{\mathcal{A}}^{VV}$ is able to detect finite-size signatures of phase transitions for comparatively small system sizes.

## DISCUSSION

We proposed the affinity susceptibility, and other measures of distance between the single particle correlations matrix, as multipurpose detectors for phase transitions where the order parameter is elusive. This situation occurs in certain systems in equilibrium but is prevalent in open systems far from equilibrium.

In contrast to the well-known fidelity susceptibility, the affinity has the advantage of being available at a lower computational cost for commonly employed numerical methods, such as Monte-Carlo and MPS techniques.

We demonstrated the usefulness and predictive power of the affinity susceptibility in two models of fermionic quantum matter out of equilibrium, sketched in Fig. 1a and b. The well-known boundary-driven fermionic chain of Fig. 1a was used as a benchmark for the proposed method while the second model allowed us to test its predictive power.

For the first model, we recovered the known phase diagram and showed that the affinity susceptibility is enhanced at the phase transition already for relatively small sizes (see Fig. 2d and e). For the boundary-driven fermionic ladder, we used the affinity to

uncover a non-trivial phase diagram. The two peak structure of the affinity susceptibility suggests the existence of two phase transitions upon increasing the interaction strength, see Fig. 3d. This is an unexpected and surprising result as all existing results for spin ladders only feature diffusive behavior[56–58].

Motivated by these results, we preformed a thorough study of the finite size scaling of the current and the spacial density profile. This corroborated the predictions of the affinity, for all numerically accessible system sizes. Our data point to the existence of two phase transitions in the thermodynamic limit, where upon increasing the interaction the systems pass from ballistic to super-diffusive and subsequently to diffusive behavior.

Another remarkable feature of the affinity susceptibility is that in all the cases we studied it signals phase transitions already for comparatively small system sizes. This suggest that corrections to scaling of the affinity susceptibility are smaller than those for other quantities. Yet, perhaps because it also encodes long-range correlations, a higher accuracy is required in the convergence of the MPO as compared to local operators like current and density. For this reason, only relatively smaller sizes were considered in the case of the ladder.

These findings underline the potential of affinity susceptibility as an indicator for phase changes in open systems.

It will be interesting to exploit the affinity to study other instances where single-particle correlators are the only easily available quantities. This applies to Quantum Monte Carlo studies out of equilibrium or at finite temperatures and in more than one dimension. Our method might also prove useful for studying time-dependent critical phenomena away from equilibrium where effective techniques are badly needed.

## METHODS

### Explicit Hamiltonians for both models

To avoid large cumbersome expressions, we presented in Eq. (5) a compressed form of the Hamiltonian and provided sketches illustrating the details of the interactions in Fig. 1a and b. For the sake of completeness, the explicit expressions for the Hamiltonian for the fermion chain model is given by

$$H = -t \sum_{r=1}^{L-1} \left[ c_r^\dagger c_{r+1} + c_{r+1}^\dagger c_r \right]$$
$$+ V \sum_{r=1}^{L-1} \left( c_r^\dagger c_r - \frac{1}{2} \right)\left( c_{r+1}^\dagger c_{r+1} - \frac{1}{2} \right), \tag{7}$$

while for the ladder

$$H = -t \sum_{r=1}^{L-1} \sum_{\tau=1,2} \left[ c_{r,\tau}^\dagger c_{r+1,\tau} + c_{r+1,\tau}^\dagger c_{r,\tau} \right]$$
$$- t \sum_{r=1}^{L} \left[ c_{r,1}^\dagger c_{r,2} + c_{r,2}^\dagger c_{r,1} \right]$$
$$+ V \sum_{r=1}^{L-1} \sum_{\tau=1,2} \left( c_{r,\tau}^\dagger c_{r,\tau} - \frac{1}{2} \right)\left( c_{r+1,\tau}^\dagger c_{r+1,\tau} - \frac{1}{2} \right)$$
$$+ V \sum_{r=1}^{L} \left( c_{r,1}^\dagger c_{r,1} - \frac{1}{2} \right)\left( c_{r,2}^\dagger c_{r,2} - \frac{1}{2} \right), \tag{8}$$

where $\tau = 1, 2$ labels the legs of the ladder.

### Properties of the single-particle affinity

In this section, we present details regarding how the single-particle affinity is numerically evaluated and discuss additional properties. In particular, we demonstrate that the affinity coincides with the mixed-state fidelity for the case of quadratic systems. This allows us to show that it satisfies the required properties of a distance between covariance matrices. Finally, we also show that

the results in the main text are expected to hold for other notions of distance between covariance matrices.

### – Details about the numerical evaluation

The affinity susceptibility is defined in terms of the expansion of the affinity, shown in Eq. (2). Defining $\mathcal{A}(\delta) = \mathcal{A}[\mathbf{\Sigma}(V), \mathbf{\Sigma}(V+\delta)]$, we can write[23,24]

$$\chi_{\mathcal{A}}^{VV}(\delta) = -\lim_{\delta \to 0} \frac{\mathcal{A}(\delta) + \mathcal{A}(-\delta) - 2\mathcal{A}(0)}{\delta^2}. \tag{9}$$

We evaluate this quantity numerically by fixing the value of the perturbation $\delta$ to be small and consider states at points $V$, $V+\delta$, and $V-\delta$. Note that, since $\Sigma$ is obtained at finite numerical precision, the value of $\delta$ has to be taken sufficiently large to ensure that the difference between the two covariance matrices is much larger than that precision.

### – Relation with fidelity for free fermions

For quadratic systems, the density operator is given by a Gaussian

$$\rho = \frac{1}{Z} e^{-\frac{1}{2}\mathbf{C}^\dagger \mathbf{\Omega C}}, \tag{10}$$

where $\mathbf{C} = \left( c_1, \cdots, c_L, c_1^\dagger, \cdots, c_L^\dagger \right)^T$ and $\mathbf{\Omega}$ is a Hermitian matrix with the particle-hole symmetric structure

$$\mathbf{\Omega} = \begin{pmatrix} \mathbf{h} & \mathbf{\Delta} \\ \mathbf{\Delta}^\dagger & -\mathbf{h}^T \end{pmatrix}. \tag{11}$$

Each of its blocks is a $L \times L$ matrix, with $\mathbf{h} = \mathbf{h}^\dagger$ and $\mathbf{\Delta}^T = -\mathbf{\Delta}$. For thermal states $\mathbf{\Omega}$ can be seen as the Hamiltonian divided by temperature. $Z$ is the partition function, which for quadratic models can be written

$$Z = \text{Tr}\left[ e^{-\frac{1}{2}\mathbf{C}^\dagger \mathbf{\Omega C}} \right] = \sqrt{\det[\mathbf{1} + e^{-\mathbf{\Omega}}]}. \tag{12}$$

The covariance matrix also acquires a simple form:

$$\mathbf{\Sigma} = \frac{1}{Z}\text{Tr}\left[ e^{-\frac{1}{2}\mathbf{C}^\dagger \mathbf{\Omega C}} \, \mathbf{C}\mathbf{C}^\dagger \right] = \left[ \mathbf{1} + e^{-\mathbf{\Omega}} \right]^{-1}. \tag{13}$$

From the definition of the fidelity

$$F(\rho_1, \rho_2) = \left( \text{Tr}\sqrt{\sqrt{\rho_1}\rho_2\sqrt{\rho_1}} \right)^2, \tag{14}$$

and using the identity

$$e^{-\frac{1}{2}\mathbf{C}^\dagger \mathbf{\Omega}_1 \mathbf{C}} e^{-\frac{1}{2}\mathbf{C}^\dagger \mathbf{\Omega}_2 \mathbf{C}} = e^{-\frac{1}{2}\mathbf{C}^\dagger \tilde{\mathbf{\Omega}} \mathbf{C}}, \tag{15}$$

where $\tilde{\mathbf{\Omega}}$ is defined as $e^{-\tilde{\mathbf{\Omega}}} = e^{-\mathbf{\Omega}_1} e^{-\mathbf{\Omega}_2}$, we can write

$$F(\rho_1, \rho_2) = \frac{1}{Z_1 Z_2}\left( \text{Tr}\sqrt{e^{-\frac{1}{2}\mathbf{C}^\dagger \mathbf{\Omega}_1 \mathbf{C}} e^{-\frac{1}{2}\mathbf{C}^\dagger \mathbf{\Omega}_2 \mathbf{C}}} \right)^2$$
$$= \frac{1}{Z_1 Z_2}\det\left[ \mathbf{1} + \sqrt{e^{-\mathbf{\Omega}_1} e^{-\mathbf{\Omega}_2}} \right] \tag{16}$$
$$= \frac{\det\left[ \mathbf{1} + \sqrt{(1 - \mathbf{\Sigma}^{-1})(2 - \mathbf{\Sigma}^{-1})} \right]}{\sqrt{\det[1 - \mathbf{\Sigma}]\det[2 - \mathbf{\Sigma}]}}$$

where $\mathbf{\Sigma}_i$ is the covariance matrix corresponding to $\rho_i$.

Note that in Eq. (16) we assumed that we can invert the covariance matrices. Nevertheless, the expression still has a well-defined value in the limit where $\mathbf{\Sigma}_i$ is not invertible.

### – Notion of distance for the single-particle affinity

A metric is a function $D: X \times X \to [0, \infty[$ that provides a distance between two members of some set $X$. It has to obey the following properties for all $x, y, z \in X$[62]:

- $D(x, y) = 0 \Leftrightarrow x = y$ identity of indiscernibles
- $D(x, y) = D(y, x)$ symmetry
- $D(x, y) \leq D(x, z) + D(z, y)$ triangle inequality.

The fidelity does not actually constitute a metric between density operators, but it can be related to other quantities that do: the Bures distance $D_{\mathcal{B}}(\rho_1, \rho_2) = \sqrt{2 - 2\sqrt{F(\rho_1, \rho_2)}}$[28–30] and the Bures angle $D_a = \arccos\sqrt{F(\rho_1, \rho_2)}$[31]. In the previous section we showed how the single-particle affinity corresponds to the fidelity for quadratic systems. By continuation, it follows that it can be related to the notion of distance between states.

### – Other notions of distance

So far we focused on the single-particle affinity and its susceptibility to detect out-of-equilibrium phase transitions. To emphasize that the quantity that contains the relevant information is the covariance matrix, we discuss here a similar analysis using different notions of distance and verify that the results agree qualitatively.

Consider the Bhattacharyya distance[63] between classical probability distributions $D_{\text{Bhatt}}(p, q) = -\log \int \sqrt{p(x)\, q(x)}\, dx$. When evaluated on Gaussian distributions with zero mean, the Bhattacharyya distance writes

$$D_{\text{Bhatt}}(p, q) = \frac{1}{2}\log\left(\frac{\det \frac{C_q + C_p}{2}}{\sqrt{\det C_q \, \det C_p}}\right), \tag{17}$$

in terms of the covariance matrices $C_p$ and $C_q$. This expression induces a distance between real covariant matrices. Its generalization to Hermitian matrices yields

$$D_{\text{Bhatt}}(\boldsymbol{\Sigma}_1, \boldsymbol{\Sigma}_2) = \frac{1}{2}\log\left(\frac{\det \frac{\boldsymbol{\Sigma}_1 + \boldsymbol{\Sigma}_2}{2}}{\sqrt{\det \boldsymbol{\Sigma}_1 \, \det \boldsymbol{\Sigma}_2}}\right). \tag{18}$$

In the same way, from the Wasserstein distance[64], we obtain

$$D_{\text{Wass}}(\boldsymbol{\Sigma}_1, \boldsymbol{\Sigma}_2) = \text{tr}\left[\boldsymbol{\Sigma}_1 + \boldsymbol{\Sigma}_2 - 2\sqrt{\sqrt{\boldsymbol{\Sigma}_2}\,\boldsymbol{\Sigma}_1\,\sqrt{\boldsymbol{\Sigma}_2}}\right]. \tag{19}$$

Finally, we also consider the Trace distance[65]

$$D_{\text{trace}}(\boldsymbol{\Sigma}_1, \boldsymbol{\Sigma}_2) = \frac{1}{2}\text{tr}\,|\boldsymbol{\Sigma}_1 - \boldsymbol{\Sigma}_2|, \tag{20}$$

where $|A| = \sqrt{A^\dagger A}$.

In Supplementary Note 1, we illustrate these different distances in the two examples considered before.

### Open systems with MPS

The vectorized form of generic density matrix $\rho_{\boldsymbol{\sigma}, \boldsymbol{\sigma}'}$, with $\boldsymbol{\sigma} = \sigma_1 \sigma_2 \ldots \sigma_L$ is given by

$$|\rho\rangle\rangle = \sum_{\boldsymbol{\sigma}, \boldsymbol{\sigma}'} \rho_{\boldsymbol{\sigma}, \boldsymbol{\sigma}'} |\boldsymbol{\sigma}, \boldsymbol{\sigma}'\rangle\rangle, \tag{21}$$

with $|\boldsymbol{\sigma}, \boldsymbol{\sigma}'\rangle\rangle = |\boldsymbol{\sigma}\rangle\langle\boldsymbol{\sigma}'|^T$. It admits the MPO decomposition

$$|\rho\rangle\rangle = \sum_{\mathbf{s}} M^{s_1} \ldots M^{s_i} \ldots M^{s_L} |\mathbf{s}\rangle. \tag{22}$$

where $s_i = (\sigma_i, \sigma_i')$, and $M^{\sigma_i, \sigma_i'}$ are the MPO decomposition matrices with dimension up to the bond dimension $D$. This yields a MPS with a local dimension encompassing the original Hilbert space and that of the copy. Using the vector notation, the integrated Lindblad dynamics of Eq. (3) is

$$|\rho(t)\rangle\rangle = e^{\hat{\mathcal{L}}t} |\rho_0\rangle\rangle. \tag{23}$$

In this form the existing time-evolution algorithms for MPS and unitary dynamics[55,66] can readily be applied here without significant modifications[33,34].

For this work we used the t-DMRG algorithm for time-evolution with a Trotter decomposition of 4th order as described in ref.[67] and with an associated error per iteration of $O(\Delta t^4)$, where $\Delta t$ is the time step.

We used the ITensor library[68] as the basis of our implementation. In the initial stages of the evolution a larger time step was chosen, typically in the range $\Delta t \in [0.1, 0.5]$, to speed up convergence. In the final stages, when necessary, we switched to a smaller time step to better approximate the steady-state, but generally not smaller than $\Delta t = 0.01$.

To guarantee the correctness of the results, the following recipe was used[69]. For a set of parameters $L$, $V$, $\eta$, and $D$,

- we monitored $J$ in the middle bond during time-evolution until it saturated. The condition for convergence was $\sigma_t/J_t < 0.01$, where $J_t$ and $\sigma_t$ are respectively the mean value and the standard deviation of the last 50 values of $J$ obtained during time-evolution for the middle bond. This ensured that fluctuations only affected digits at least two decimal places after the most significant one;
- the obtained steady-states are supposed to possess a constant current across the length of the system, which was tracked by checking if $\sigma_x/J_x < 0.01$, where $J_x$ and $\sigma_x$ are the mean value and standard deviation for the current at the different bonds. If this condition was not fulfilled, the state was evolved further in time until it was;
- to determine if the MPO description approximates sufficiently well a given steady-state, we also analyzed the convergence with bond dimension. The criterion for convergence of the current with bond dimension, which was applied for prototypical cases, was $\sigma_D/J_D < 0.01$, where $J_D$ and $\sigma_D$ are respectively the mean value and standard deviation of a set composed of $J_x$, for the largest bond dimensions used. Typically, the bond dimension of the results shown in the main text was $D = 100$, but it went up to $D = 150$ for the larger system sizes.

## DATA AVAILABILITY

## CODE AVAILABILITY

## REFERENCES
1. Sachdev, S. *Quantum Phase Transitions* 2nd edn (Cambridge University Press, Cambridge, 2011).
2. Osterloh, A., Amico, L., Falci, G. & Fazio, R. Scaling of entanglement close to a quantum phase transition. *Nature* **416**, 608–610 (2002).
3. GU, S.-J. Fidelity approach to quantum phase transitions. *Int. J. Mod. Phys. B* **24**, 4371–4458 (2010).
4. Morrison, S. & Parkins, A. S. Dynamical quantum phase transitions in the dissipative lipkin-meshkov-glick model with proposed realization in optical cavity QED. *Phys. Rev. Lett.* **100**, 040403 (2008).
5. Höning, M., Moos, M. & Fleischhauer, M. Critical exponents of steady-state phase transitions in fermionic lattice models. *Phys. Rev. A* **86**, 013606 (2012).
6. Lee, T. E., Chan, C.-K. & Yelin, S. F. Dissipative phase transitions: indepen dent versus collective decay and spin squeezing. *Phys. Rev. A* **90**, 052109 (2014).
7. Genway, S., Li, W., Ates, C., Lanyon, B. P. & Lesanovsky, I. Generalized Dicke nonequilibrium dynamics in trapped ions. *Phys. Rev. Lett.* **112**, 023603 (2014).

8. Manzano, D. & Hurtado, P. I. Symmetry and the thermodynamics of currents in open quantum systems. *Phys. Rev. B* **90**, 125138 (2014).

9. Wilming, H., Kastoryano, M. J., Werner, A. H. & Eisert, J. Emergence of spontaneous symmetry breaking in dissipative lattice systems. *J. Math. Phys.* **58**, 033302 (2017).

10. Sánchez Muñoz, C. et al. Symmetries and conservation laws in quantum trajectories: dissipative freezing. *Phys. Rev. A* **100**, 042113 (2019).

11. Ferreira, J. S. & Ribeiro, P. Lipkin-meshkov-glick model with markovian dissipation: a description of a collective spin on a metallic surface. *Phys. Rev. B* **100**, 184422 (2019).

12. Huber, J., Kirton, P. & Rabl, P. Phase-space methods for simulating the dissipative many-body dynamics of collective spin systems. *SciPost Phys.* **10**, 45 (2021).

13. Kessler, E. M. et al. Dissipative phase transition in a central spin system. *Phys. Rev. A* **86**, 012116 (2012).

14. Puel, T. O., Chesi, S., Kirchner, S. & Ribeiro, P. Mixed-order symmetry-breaking quantum phase transition far from equilibrium. *Phys. Rev. Lett.* **122**, 235701 (2019).

15. Hannukainen, J. & Larson, J. Dissipation-driven quantum phase transitions and symmetry breaking. *Phys. Rev. A* **98**, 042113 (2018).

16. Huber, J., Kirton, P. & Rabl, P. Nonequilibrium magnetic phases in spin lattices with gain and loss. *Phys. Rev. A* **102**, 012219 (2020).

17. Khemani, V., Lazarides, A., Moessner, R. & Sondhi, S. L. Phase structure of driven quantum systems. *Phys. Rev. Lett.* **116**, 250401 (2016).

18. Else, D. V., Bauer, B. & Nayak, C. Floquet time crystals. *Phys. Rev. Lett.* **117**, 090402 (2016).

19. Ribeiro, P., Zamani, F. & Kirchner, S. Steady-state dynamics and effective temperature for a model of quantum criticality in an open system. *Phys. Rev. Lett.* **115**, 220602 (2015).

20. Zanardi, P., Quan, H. T., Wang, X. & Sun, C. P. Mixed-state fidelity and quantum criticality at finite temperature. *Phys. Rev. A* **75**, 032109 (2007).

21. Zanardi, P., Campos Venuti, L. & Giorda, P. Bures metric over thermal state manifolds and quantum criticality. *Phys. Rev. A* **76**, 062318 (2007).

22. Cozzini, M., Ionicioiu, R. & Zanardi, P. Quantum fidelity and quantum phase transitions in matrix product states. *Phys. Rev. B* **76**, 104420 (2007).

23. Rossini, D. & Vicari, E. Ground-state fidelity at first-order quantum transitions. *Phys. Rev. E* **98**, 062137 (2018).

24. Mera, B., Vlachou, C., Paunković, N., Vieira, V. R. & Viyuela, O. Dynamical phase transitions at finite temperature from fidelity and interferometric loschmidt echo induced metrics. *Phys. Rev. B* **97**, 094110 (2018).

25. Penrose, O. & Onsager, L. Bose-Einstein condensation and liquid helium. *Phys. Rev.* **104**, 576–584 (1956).

26. Bera, S., Schomerus, H., Heidrich-Meisner, F. & Bardarson, J. H. Many-body localization characterized from a one-particle perspective. *Phys. Rev. Lett.* **115**, 046603 (2015).

27. Bera, S., Martynec, T., Schomerus, H., Heidrich-Meisner, F. & Bardarson, J. H. One-particle density matrix characterization of many-body localization. *Ann. Phys.* **529**, 1600356 (2017).

28. Bures, D. An extension of Kakutani's theorem on infinite product measures to the tensor product of semifinite $w^*$-algebras. *Trans. Am. Math. Soc.* **135**, 199–212 (1969).

29. Uhlmann, A. The "transition probability" in the state space of a $\star$-algebra. *Rep. Math. Phys.* **9**, 273–279 (1976).

30. Jozsa, R. Fidelity for mixed quantum states. *J. Mod. Opt.* **41**, 2315–2323 (1994).

31. Uhlmann, A. Geometric phases and related structures. *Rep. Math. Phys.* **36**, 461–481 (1995).

32. Landi, G. T., Poletti, D. & Schaller, G. Non-equilibrium boundary driven quantum systems: models, methods and properties. *Rev. Mod. Phys.* **94**, 045006 (2022).

33. Zwolak, M. & Vidal, G. Mixed-state dynamics in one-dimensional quantum lattice systems: a time-dependent superoperator renormalization algorithm. *Phys. Rev. Lett.* **93**, 207205 (2004).

34. Verstraete, F., García-Ripoll, J. J. & Cirac, J. I. Matrix product density operators: Simulation of finite-temperature and dissipative systems. *Phys. Rev. Lett.* **93**, 207204 (2004).

35. Rams, M. M. & Zwolak, M. Breaking the entanglement barrier: tensor network simulation of quantum transport. *Phys. Rev. Lett.* **124**, 137701 (2020).

36. Gullans, M. J. & Huse, D. A. Entanglement structure of current-driven diffusive fermion systems. *Phys. Rev. X* **9**, 021007 (2019).

37. Cubitt, T. S., Lucia, A., Michalakis, S. & Perez-Garcia, D. Stability of local quantum dissipative systems. *Commun. Math. Phys.* **337**, 1275–1315 (2015).

38. Brandão, F., Cubitt, T. S., Lucia, A., Michalakis, S. & Perez-Garcia, D. Area law for fixed points of rapidly mixing dissipative quantum systems. *J. Math. Phys.* **56**, 102202 (2015).

39. Prosen, T. & Žnidarič, M. Matrix product simulations of non-equilibrium steady states of quantum spin chains. *J. Stat. Mech. Theory Exp.* **2009**, P02035 (2009).

40. Benenti, G., Casati, G., Prosen, T. & Rossini, D. Negative differential conductivity in far-from-equilibrium quantum spin chains. *EPL* **85**, 37001 (2009).

41. Benenti, G., Casati, G., Prosen, T., Rossini, D. & Žnidarič, M. Charge and spin transport in strongly correlated one-dimensional quantum systems driven far from equilibrium. *Phys. Rev. B* **80**, 035110 (2009).

42. Žnidarič, M. Dephasing-induced diffusive transport in the anisotropic Heisenberg model. *New J. Phys.* **12**, 043001 (2010).

43. Prosen, T. & Žnidarič, M. Long-range order in nonequilibrium interacting quantum spin chains. *Phys. Rev. Lett.* **105**, 060603 (2010).

44. Žnidarič, M. Spin transport in a one-dimensional anisotropic heisenberg model. *Phys. Rev. Lett.* **106**, 220601 (2011).

45. Žnidarič, M. Transport in a one-dimensional isotropic Heisenberg model at high temperature. *J. Stat. Mech. Theory Exp.* **2011**, P12008 (2011).

46. Mendoza-Arenas, J. J., Grujic, T., Jaksch, D. & Clark, S. R. Dephasing enhanced transport in nonequilibrium strongly correlated quantum systems. *Phys. Rev. B* **87**, 235130 (2013).

47. Mendoza-Arenas, J. J., Al-Assam, S., Clark, S. R. & Jaksch, D. Heat transport in the XXZ spin chain: from ballistic to diffusive regimes and dephasing enhancement. *J. Stat. Mech: Theory Exp.* **2013**, P07007 (2013).

48. Žnidarič, M. Exact solution for a diffusive nonequilibrium steady state of an open quantum chain. *J. Stat. Mech. Theory Exp.* **2010**, L05002 (2010).

49. Žnidarič, M. Solvable quantum nonequilibrium model exhibiting a phase transition and a matrix product representation. *Phys. Rev. E* **83**, 011108 (2011).

50. Prosen, T. Open XXZ spin chain: nonequilibrium steady state and a strict bound on ballistic transport. *Phys. Rev. Lett.* **106**, 217206 (2011).

51. Prosen, T. Exact nonequilibrium steady state of a strongly driven open XXZ chain. *Phys. Rev. Lett.* **107**, 137201 (2011).

52. Prosen, T. Matrix product solutions of boundary driven quantum chains. *J. Phys. A: Math. Theor.* **48**, 373001 (2015).

53. Breuer, H.-P. & Petruccione, F. *The Theory of Open Quantum Systems* 1st edn (Oxford University Press, 2002).

54. Gardiner, C. & Zoller, P. *Quantum Noise: A Handbook of Markovian and Non-Markovian Quantum Stochastic Methods with Applications to Quantum Optics.* 2nd edn (Springer, 2000).

55. Daley, A. J., Kollath, C., Schollwöck, U. & Vidal, G. Time-dependent density-matrix renormalization-group using adaptive effective hilbert spaces. *J. Stat. Mech: Theory Exp.* **2004**, P04005 (2004).

56. Žnidarič, M. Coexistence of diffusive and ballistic transport in a simple spin ladder. *Phys. Rev. Lett.* **110**, 070602 (2013).

57. Žnidarič, M. Magnetization transport in spin ladders and next-nearest-neighbor chains. *Phys. Rev. B* **88**, 205135 (2013).

58. Prosen, T. & Žnidarič, M. Diffusive high-temperature transport in the one-dimensional Hubbard model. *Phys. Rev. B* **86**, 125118 (2012).

59. Prosen, T. Exact nonequilibrium steady state of an open Hubbard chain. *Phys. Rev. Lett.* **112**, 030603 (2014).

60. Popkov, V. & Prosen, T. Infinitely dimensional lax structure for the one-dimensional Hubbard model. *Phys. Rev. Lett.* **114**, 127201 (2015).

61. Steinigeweg, R., Heidrich-Meisner, F., Gemmer, J., Michielsen, K. & De Raedt, H. Scaling of diffusion constants in the spin-$\frac{1}{2}$ XX ladder. *Phys. Rev. B* **90**, 094417 (2014).

62. Bengtsson, I. & Życzkowski, K. *Geometry of Quantum States an Introduction to Quantum Entanglement*. 2nd edn (Cambridge University Press, 2017).

63. Kailath, T. The divergence and Bhattacharyya distance measures in signal selection. *IEEE Trans. Commun. Technol.* **15**, 52–60 (1967).

64. Dowson, D. & Landau, B. The fréchet distance between multivariate normal distributions. *J. Multivar. Anal.* **12**, 450–455 (1982).

65. Michael A. Nielsen, I. L. C. *Quantum Computation and Quantum Information* 10th edn (Cambridge University Press, 2011).

66. Vidal, G. Efficient simulation of one-dimensional quantum many-body systems. *Phys. Rev. Lett.* **93**, 040502 (2004).

67. Prosen, T. & Pižorn, I. High order non-unitary split-step decomposition of unitary operators. *J. Phys. A: Math. Gen.* **39**, 5957–5964 (2006).

68. Fishman, M., White, S. R. & Stoudenmire, E. M. The ITensor software library for tensor network calculations. *SciPost Phys. Codebases* 4 (2022).

69. Ferreira, J. S. & Filippone, M. Ballistic-to-diffusive transition in spin chains with broken integrability. *Phys. Rev. B* **102**, 184304 (2020).

## ACKNOWLEDGEMENTS

## COMPETING INTERESTS

The authors declare no competing interests.

## ADDITIONAL INFORMATION

**Supplementary information** The online version contains supplementary material available at https://doi.org/10.1038/s41534-022-00671-8.

**Correspondence** and requests for materials should be addressed to Miguel M. Oliveira, Pedro Ribeiro or Stefan Kirchner.

**Reprints and permission information** is available at http://www.nature.com/reprints

**Publisher's note** Springer Nature remains neutral with regard to jurisdictional claims in published maps and institutional affiliations.